

1 **Manifestations of syn-eruptive fluid circulations on carbonate veins, Central Anatolian**

2 **Volcanic Province**

3

4 Volkan Karabacak<sup>a\*</sup>, Halim Mutlu<sup>b</sup>, Kıymet Deniz<sup>b</sup>

5 <sup>a</sup> Department of Geological Engineering, Eskisehir Osmangazi University, Eskisehir, Turkey

6 <sup>b</sup> Department of Geological Engineering, Ankara University, Ankara, Turkey

7

8

9

10 \*corresponding author:

11 Professor Volkan Karabacak, PhD  
12 Eskişehir Osmangazi University,  
13 Department of Geological Engineering,  
14 26040, Eskişehir, Turkey  
15 *Fax:* +90 222 2290535,  
16 *Phone:* +90 222 2393750/3408,  
17 *e-mail:* karabacak@ogu.edu.tr

18

19

20 ***Keywords:*** volcanism, carbonate vein, eruption, dating, central Anatolia

21

22

23

24

## 25 **Abstract**

26 Although there are several attempts to compare the age distributions on travertines with episodes of  
27 surrounding volcanism, the correlation between the precipitation record of carbonate veins and the  
28 fractural pattern around a volcanic conduit has not yet been examined. In this study, we investigate  
29 the geochronological, geochemical and isotopic characteristics of two travertine deposits (Balkaya  
30 and Sarıhıdır) surrounded by many eruption centers in the central Anatolia with ample paleoeruption  
31 records. High-resolution carbonate precipitation records revealed by U-series dating are well  
32 correlated with the compiled dataset on Acıgöl caldera and Erciyes stratovolcano eruptions with  
33 regard to fractural positioning to the volcanic centers. Syn-eruptive carbonate precipitation is  
34 thought to occur because of sudden flux of CO<sub>2</sub>-rich fluid along the extensional fracture systems  
35 aligned tangential to the related volcanic conduit and, therefore, may be an alternative technique for  
36 the reconstruction of paleoeruptions.  $\delta^{18}\text{O}$  and  $\delta^{13}\text{C}$  values of the travertine sites are within the  
37 range of meteogene fluids and  $\delta^{18}\text{O}$  values show a similar trend to climate proxies preserved in  
38 different depositional environments throughout the world. It is likely due to that studied  
39 carbonates were precipitated under similar fluid conditions which are represented by high  
40 rate of dilatation followed by the meteoric water influx into the extensional fracture systems.

41

42

## 43 **1. Introduction**

44 The internal structure of thermogenic carbonate veins is composed of alternated vertical  
45 bands that are precipitated from CO<sub>2</sub>-rich hot waters through the fracture systems around  
46 the geothermal areas (Pentocost, 2005; Uysal et al., 2007; Brogi and Capezzuoli, 2014;  
47 Karabacak et al., 2017). The formation of these bands is closely linked to repeated

48 precipitation episodes that require reopening of previously sealed fractures within the  
49 bedrock, favouring a temporary hydrothermal fluid circulation. Every band of the vein  
50 presents a limited time that corresponds to the period starting just after the event until  
51 sealing (Williams et al., 2017; Capezzuoli et al., 2018; Karabacak et al., 2019). Thus, since  
52 carbonate veins are highly suitable for direct dating of calcite, they provide an opportunity  
53 to understand the history of fluid circulation in a region of seismic or volcanic unrest.

54 Most of the previous studies devoted to carbonate veins focus on the interaction with fluid  
55 circulation and active crustal deformation (e.g. type and direction of regional stresses,  
56 dilatational rate) (e.g. Altunel and Karabacak, 2005; Uysal et al., 2007; Brogi et al., 2017). In  
57 recent works, their relations with earthquake strain cycles are also addressed (Uysal et al.,  
58 2011; Brogi and Capezzuoli, 2014; Williams et al., 2017). Moreover, it is proven that the age  
59 distributions of vertical bands in a carbonate vein supply direct dates of the nearby fluid flow  
60 circulation in the areas of seismic unrest (Karabacak et al., 2019). These features make the  
61 carbonate veins quite attractive for the active tectonic studies.

62 In volcanic regions, deformation is caused by shear failure, tensile failure or fluid  
63 pressurization process that produce ruptures at the tip of a magma body during strain cycles  
64 (Anderson, 1951; Rubin and Gillard, 1998; Azzarro, 1999; Glen and Ponce, 2002; Zobin,  
65 2003). Stress in a radial-pattern spreading generates extensional fractures positioned  
66 tangential to volcanic conduits (e.g. Anderson, 1951; Macdonald, 1972; Park, 1989; Borgia et  
67 al., 2014) thus creating deep migration pathways for the fluids. During strain cycles, changes  
68 may also occur in deep aquifers (Montgomery and Manga, 2003; Wang et al., 2004) that are  
69 loaded by great elastic strain at depth (Seed and Idriss 1971), resulting in a relatively large  
70 expulsion of depressurized CO<sub>2</sub>-rich hot waters. Therefore, subsurface hot fluids are

71 mobilized in deeply penetrating fractures that act as conduits for hot waters and as a result,  
72 carbonates are precipitated around the volcanic eruption centers.

73 The previous studies asserted the temporal correlation between carbonate precipitation and  
74 volcanism with random sampling strategies on travertine deposits, carbonate veins and  
75 speleotherms (e.g. Tuccimei et al., 2006; Priewisch et al., 2014; Karabacak et al., 2017;  
76 Weinstein et al., 2020). For example, Priewisch et al. (2014) suggest that the deposition ages  
77 of voluminous travertines overlap with the episodes of basaltic volcanism in New Mexico  
78 and Arizona. Karabacak et al. (2017) compare U-series geochronology of carbonate veins  
79 with previous volcanic eruption records and achieve to resolve independent events on two  
80 different eruption centers. In the literature, however, there is a lack of studies focusing on  
81 continuous precipitation record to compare the syn-eruptive fluid circulations and carbonate  
82 vein ages. Furthermore, none of the previous studies assessed the correlations regarding the  
83 fractural pattern and volcanic conduit position.

84 In this study, we investigate a continuous precipitation records of carbonate veins in the  
85 Central Anatolian Volcanic Province (CAVP) and evaluate precise U-Th ages, mineralogy, and  
86 geochemical and isotopic characteristics of alternated bands. We compare our results with  
87 paleo-eruption records from major volcanic centers (Figure 1). Our correlations are  
88 discussed with regard to fractural positioning to the eruption centers to discriminate the  
89 event origin. Furthermore, oxygen isotope and rare element compositions of vein samples  
90 provided us with a great opportunity to examine temporal variations in the temperature and  
91 source of fluids that precipitated the studied travertines in the region.

92

93

94 **2. Material and Method**

95 Mineralogical and petrographic determinations of carbonate samples were carried out at the  
96 Geology Department (YEBIM Center) of the Ankara University. Porosity types and textural  
97 characteristics of samples were studied with Leica DMLP model polarizing microscope.

98 Mineralogical composition of carbonates was determined with Inel Equinox 1000 X-Ray  
99 Diffractometer. Raman spectroscopy analysis on selected samples was conducted with DXR  
100 brand using laser beam of 780 nm.

101 Carbon and oxygen isotope analyses of carbonate samples were carried out with micromass  
102 Isoprime dual inlet isotope ratio mass spectrometer (DI-IRMS) at the Environmental Isotope  
103 Laboratory of the University of Arizona. Samples were reacted with dehydrated phosphoric  
104 acid ( $\text{H}_3\text{PO}_4$ ) under vacuum at a temperature of  $70^\circ\text{C}$ . The isotope ratio measurement is  
105 calibrated based on replicate measurements of international standards NBS-19 and NBS-18.  
106 The analytical precision is  $\pm 0.1\%$  for  $\delta^{18}\text{O}$  and  $\pm 0.08\%$  for  $\delta^{13}\text{C}$  ( $1\sigma$ ).

107 The trace element analyses of the carbonate samples were performed at the Radiogenic  
108 Isotope Laboratory, the University of Queensland on a Thermo X-series ICP-MS with  
109 instrument conditions as described in Lawrence and Kamber (2006), after dissolving the  
110 carbonates in a 2%  $\text{HNO}_3$  solution embed with internal standards. The raw data were  
111 corrected for the low, detectable blank, internal and external drift, and for oxides and  
112 doubly charged species. Instrument response was calibrated against two independent  
113 digests of the USGS reference W-2, and confirmed by analysis of other inter-lab references,  
114 treated as unknowns. Corrections were applied for oxides using formation rates determined  
115 from pure single element REE standards.

116 Carbonate samples were dated by U-series technique at the Radiogenic Isotope Laboratory  
117 at the University of Queensland using a Nu Plasma HR Multicollector Inductively Coupled  
118 Plasma Mass Spectrometer (MCICP- MS) following the analytical protocols described in Zhao  
119 et al. (2001) and Ünal-İmer et al. (2016).  $^{230}\text{Th}/^{238}\text{U}$  and  $^{234}\text{U}/^{238}\text{U}$  ratios were calculated  
120 using decay constants given by Cheng et al. (2000). U-series ages were estimated using the  
121 DensityPlotter 8.5 (Vermeesch, 2012).

122

123

### 124 **3. Geological Setting**

#### 125 **3.1. Central Anatolian Volcanic Province**

126 The tectonics of the Anatolian Block is governed by interactions between three major plates;  
127 African, Arabian and Eurasian plates. Owing to this outstanding location, the Anatolian block  
128 represents an intraplate deformation resulting from the northward convergence of the Afro-  
129 Arabian plates to the Eurasian plate. As commonly expected within intraplate domains  
130 controlled by collisional margins, the central part of Anatolia has witnessed an intense  
131 Neogene-Quaternary volcanic activity associated mainly with subduction events (Innocenti  
132 et al., 1975; Aydar et al., 1994; 1995; Piper et al., 2002).

133 The central Anatolia is shaped by a triangular frame controlled by Quaternary faults; NW-SE-  
134 trending Tuzgölü Fault Zone (TFZ) in the west, NE-SW-trending Ecemiş Fault Zone (EFZ) in the  
135 east and the Central Kızılırmak Fault Zone (CKFZ) in the north. The TFZ and EFZ consist of  
136 Holocene faults with strike-slip component (Dirik and Göncüoğlu, 1996; Emre et al., 2011).  
137 The CKFZ present a southward arc-shape geometry through the Kızılırmak River (Toprak,

138 1994). It consists of Quaternary normal faults and linements of faults with strike-slip  
139 component (Dirik and Göncüoğlu, 1996; Emre et al., 2011) and constitutes the northern margin  
140 of the CAVP (Toprak, 1994). The region of triangular frame, so called the CAVP, is surrounded  
141 by a number of eruption centers such as major composite volcanoes and monogenetic cones  
142 with voluminous volcanic products (Toprak and Göncüoğlu, 1993). In this province,  
143 Quaternary eruption development has been controlled by three main eruption centers  
144 (Acıgöl caldera, Hasandag and Erciyes stratovolcanoes) within an area of 40 km radius.  
145 Hasandağ and Erciyes composite volcanoes were formed along the TFZ and EFZ (Pasquare et  
146 al., 1988; Toprak and Göncüoğlu, 1993). The Acıgöl Caldera area lies in the central part by  
147 monogenetic cones. Paleoeruption events on extrusive materials in the region were dated  
148 by a range of methods (for the last 190 ka) (Table S1).

149

### 150 **3.2. Balkaya and Sarıhıdır travertine sites**

151 In the current study, we focus on fracture systems and their carbonate veins in Balkaya and  
152 Sarıhıdır travertine sites around the Avanos town that is surrounded by well-known volcanic  
153 centers between the Acıgöl caldera and Erciyes stratovolcano. In the area, Kızılırmak River  
154 flows towards west by drawing a southward arc.

155 Figure 2 presents the geological setting of the study area that was improved from Köksal and  
156 Göncüoğlu (1997) and Koçyiğit and Doğan (2016) authors' field observations. In the study  
157 area, Mesozoic-aged metamorphites (Köksal and Göncüoğlu, 1997) comprise the basement  
158 and are overlain by the Upper Cretaceous-Lower Paleocene granitoid-syenitoid and Middle-  
159 Upper Eocene limestones (Koçyiğit and Doğan, 2016). Volcaniclastic sediments consisting of  
160 tuffaceous fluvial deposits (Upper Miocene-Pliocene) form a huge platform at the south of

161 Kızılırmak River and become thinner to the north (Köksal and Göncüoğlu, 1997; Koçyiğit and  
162 Doğan, 2016). The Upper Miocene-Lower Pleistocene fluvial and lacustrine deposits are  
163 represented by tectonically controlled margins and lie on the hanging walls of the normal  
164 faults (Koçyiğit and Doğan, 2016). The studied travertines are exposed as separate bodies at  
165 the Sarıhıdır and Balkaya sites in northern part of the Avanos town.

166

### 167 **3.3. Syntectonic fluid circulation**

168 During seismic release, deep aquifers are loaded by larger elastic strain which causes a  
169 relatively huge expulsion of depressurized CO<sub>2</sub>-rich hot waters (Montgomery and Manga,  
170 2003; Wang et al., 2004; Berardi et al., 2016; Karabacak et al., 2017) giving rise to carbonate  
171 precipitation within fractures that serve as conduits for CO<sub>2</sub>-charged groundwater (Sibson,  
172 1987; Altunel and Karabacak, 2005). Although both high flux of CO<sub>2</sub> and large rate of  
173 groundwater discharge are the ultimate drivers of carbonate vein precipitation in deeply-  
174 penetrating fractures, climate-driven near-surface hydrological changes may also play an  
175 important role in episodic CO<sub>2</sub>-rich fluid circulation. Recent studies have shown that the  
176 timing of vein formation coincides preferentially with colder and drier climate regimes (Uysal  
177 et al., 2019). Such carbonate vein precipitation is, therefore, a direct record of the seismic  
178 release during glacial periods (Uysal et al., 2007; 2011; Brogi and Capezzuoli, 2014).

179 The internal structure of carbonate veins formed in alternated bands is closely linked to  
180 repeated crustal reactivation that requires fluid circulation (Uysal et al., 2007; Nuriel et al.,  
181 2012; Brogi and Capezzuoli, 2014; Karabacak et al., 2017; Williams et al., 2017). Karabacak et  
182 al. (2019) review the cycles of banded carbonate vein precipitation in tectonically active  
183 areas (Table 1) and suggest that 1) *coseismic period* involves the opening/reopening of

184 fractures due to seismic release. Simultaneous fluid circulation in fracture systems and  
185 expulsion of depressurized/supersaturated hot water are resulted in rapid precipitation of  
186 carbonates on both walls of the fracture (planar). The band is formed as whitish  
187 microcrystalline calcite that is related to abundant fluid inclusions with high-CO<sub>2</sub> degassing,  
188 2) during the *post-seismic period*, saturated fluids still discharge with relatively slow flow  
189 rate until the fracture is completely plugged. Because of slow degassing rates, light-  
190 transparent macrocrystalline calcites are precipitated and 3) until the next seismic event no  
191 more carbonate could be precipitated under slow-flowing conditions. This *interseismic*  
192 *period* forms a hiatus with the former carbonate band.

193

194

## 195 **4. Results**

### 196 **4.1. Sampling**

197 We investigated the structural features reported in the previous studies in the neighborhood  
198 of study area (i.e. Toprak, 1994; Köksal and Göncüoğlu, 1997; Emre et al., 2011a; 2011b;  
199 Koçyiğit and Doğan, 2016) using digital elevation data at ca. 29-m ground pixel resolutions  
200 (AsterGDEM v2) (Figures 1, 2 and S1). The key morphological lineaments were determined  
201 by satellite images (from Google Earth software) and confirmed by field observations (Figure  
202 2). Accordingly, main lineaments controlling the northern margin of the Kızılırmak valley are  
203 found to extend in E-W direction with a southward arc-shape geometry.

204 There are two travertine sites (Balkaya and Sarıhıdır) formed on these lineaments in a few  
205 km distance. Balkaya travertines occur on a dilational jog between the NW-SE-trending dip-

206 slip faults with length of about 3 km (Figures 2 and S1b). They display a normal fault  
207 morphology on which the southern blocks have moved downward. Travertines with a well-  
208 protected morphology, consist of a main central fissure filled with carbonate vein (vertically  
209 banded compact travertines), and porous bedded travertines dipping away from the central  
210 fissures. Fracture analyses on carbonate veins show the presence of two dominant stress  
211 orientations spanning the range of  $70^\circ$  to  $130^\circ$  (Figure 2). They are controlled by two  
212 conjugated sets displaying a hybrid fracture feature.

213 The Sarihıdır travertines are formed on a jogging area between a NE-SW-trending left-lateral  
214 oblique fault and a NE-SW-trending morphological lineament (Figures 2 and S1a). Most of  
215 the fissures in this site have been filled with carbonate material. Field observations and bi-  
216 directional rose diagrams plotted for the Sarihıdır fissures and veins reveal two conjugate  
217 sets in a range of  $40^\circ$  to  $120^\circ$  (Figure 2).

218 For isotopic and geochemical analyses, using microdrilling technique we sampled 36 bands  
219 from four selected carbonate veins at Sarihıdır (locations 1 and 2) and Balkaya (locations 3  
220 and 4) sites (Table S2, Figures S1-4). We selected veins that are suitable for sampling across  
221 their entire width (wall to wall) or at least from wall to the fissure center. The sampling  
222 strategy is focused on relatively thick, detritus-free crystalline bands along the veins. All  
223 samples were labelled and signed onsite to indicate the first precipitation sides.

224

#### 225 **4.2. Mineralogical and petrographic analyses**

226 Carbonate band samples were cut parallel to their deposition directions. The samples were  
227 polished and cleaned ultrasonically. Before the analysis, two sets were prepared: one of the

228 sets was used to investigate the whole rock mineralogy and microtexture by XRD and  
229 another was for thin section petrography.

230 Carbonate samples from the Balkaya and Sarıhıdır locations are divided into several  
231 subgroups concerning their textural features and mineral sizes (Table S3, Figures S5-S8). The  
232 first subgroup of the Balkaya samples is represented by well-developed banded and flow  
233 textures and composed chiefly of idiomorph, coarse crystalline, needle-shaped calcite  
234 minerals accompanied by trace amount of kaolinite (Figure S5a, b). Results of confocal  
235 Raman spectroscopic (CRS) and electron probe microanalysis (EPMA) studies indicate that  
236 bands are made up of rhodochrosite (Figure S7) and cryptocrystalline quartzs comprise the  
237 porous parts of carbonates. The porosity type is burrowing. The second subgroup of Balkaya  
238 samples has granular (mosaic) texture with different sized xenomorphic calcite minerals  
239 (Figure S5c, d) represented by fenestral type porosity. The third group is comprised by both  
240 flow and granular textures with shelter porosity (Figure S5e, f). The fourth group shows fine  
241 crystalline granular texture with shelter and fenestral porosity (Figure S5g, h). Balkaya  
242 carbonates are formed within the cracks and fractures of micritic limestone, which consists  
243 of calcite with rare quartz. The existence of quartz may indicate occasional erosion and  
244 sediment transport by surface runoff to the deposition site.

245 Concerning texture types, the Sarıhıdır samples are divided into three subgroups. The first  
246 group has finely banded (flow) and granular textures and consists of fine to coarse crystalline  
247 calcite with rare quartz, pyroxene (augite), epidote and clay minerals (Figure S6a, b and S8).  
248 They typically have shelter type porosity. The second group of carbonates is characterized by  
249 finely crystalline granular texture and shelter type porosity (Figure S6c, d). Samples of this  
250 group are composed of calcite, quartz, feldspar (bytownite) and opaque minerals

251 (manganese dioxide) (Figure S6c, d and S8). The third group presents very finely banded and  
252 well-developed flow textures with shelter and fenestral type porosity (Figure S6e-h). Clay  
253 minerals occur in the carbonate bands.

254 Idiomorph and coarsely crystalline, needle-shaped calcites indicate rapid crystallization from  
255 the fluid. Coarse crystalline calcite minerals grow toward the fluid direction whereas fine  
256 crystalline calcites point to crystallization under a stagnant flow regime (Rizzo et al., 2019).  
257 Because of heterogeneous crystallization, calcites show various crystal sizes. The flow rate of  
258 fluids forming this subgroup is quite varied. Sarıhıdır samples contain mineral fragments of  
259 volcanic or intrusive rocks exposed in the study area. The banded texture of Balkaya  
260 carbonates is much better developed than the Sarıhıdır samples and Mn-bearing bands are  
261 thicker for the former. Cataclastic texture recognized within the Sarıhıdır carbonate veins  
262 indicates that seismic event probably postdates the carbonate formation.

263

#### 264 **4.3. U-Th geochronology**

265 Based on the results of XRD and microscopy studies, collected carbonate samples are  
266 coarsely crystalline and consist of almost 100% calcite minerals. Calcite fabrics are generally  
267 observed as long elongated and open columnar forms. The discontinuities between the  
268 bands (hiatus) are quite noticeable ensuring no contamination in adjacent generations  
269 (Figure 3). Most of the bands display two crystalline zones: 1) towards fracture wall, whitish  
270 microcrystalline calcites that are related to abundant fluid inclusions with high-CO<sub>2</sub>  
271 degassing, 2) towards fracture center, light-transparent macrocrystalline calcites that are  
272 related to slow degassing rates. For U-Th dating, carbonate vein bands were microdrilled

273 from the whitish microcrystalline parts, immediate nearest location of the band to the  
274 fracture wall (Figure 3).

275  $^{230}\text{Th}/^{232}\text{Th}$  ratios of most samples (more pronounced for the Sarıhıdır samples) are lower  
276 than 10 showing the presence of detrital  $^{232}\text{Th}$  in Balkaya and Sarıhıdır sites (Tables 2 and  
277 S4). The samples have very low U contents (6.6 to 37.4 ppb). This may imply that there might  
278 be a time gap between the vein formation and the commencement of carbonate  
279 crystallization, which led to clastic material to accommodate at the deposition site.

280 Regarding Sarıhıdır carbonates, U-Th dates of location 1 vary from 7.5 to 29 ka and those of  
281 location 2 are rather older and range from 66 to 82 ka within analytical errors. Location 3  
282 from the Balkaya site yields U/Th ages in the range of 33 to 73 ka. Location 4 at this site gives  
283 a wide range of age data from 14.9 to 171 ka.

284

#### 285 **4.4. Rare earth element contents**

286 Rare earth element + Y contents of studied travertine samples are shown in Table S5. Total  
287 REY of samples fall in a wide range from 176 to 23509 ppb. REY contents of Balkaya  
288 travertines (2.4 to 23.5 ppm) are significantly higher than those of Sarıhıdır travertines (0.2  
289 to 2.1 ppm). REY patterns of both sample sets are 1 to 3 orders of magnitude lower than the  
290 PAAS (Post-Archean Australian Shale) values (Taylor and McLennan, 1985) (Figure 4a). REY  
291 concentrations of Balkaya samples steeply descend from La to Y and continue with a nearly  
292 flat pattern across the HREEs. However, REY patterns of Sarıhıdır travertines maintain a  
293 horizontal position from La to Lu, except for a sharp positive Eu anomaly, which might be  
294 due to replacement of calcium by this element (e.g. Rankama and Sahama, 1950).

295 In the PAAS-normalized diagram, REY contents of Balkaya and Sarıhıdır travertines are  
296 compared to those of volcanic and granitoid rocks exposing in the region (Toksoy-Köksal et  
297 al., 2008). It is shown that host rocks with REY concentrations greater than travertines  
298 display a flat trend that slightly descends from La to Lu.

299

#### 300 **4.5. Stable isotopes**

301  $\delta^{18}\text{O}$  and  $\delta^{13}\text{C}$  values of Balkaya and Sarıhıdır samples are given in Table 2. Carbon isotope  
302 composition of Balkaya carbonates is in the range of 11.5 to 13.2‰ (VPDB) and those of  
303 Sarıhıdır carbonates varies from 8.7 to 11.0‰ (VPDB). Oxygen isotope values of Balkaya and  
304 Sarıhıdır samples are from -11.6 to -9.5‰ (VPDB) and from -16.2 to -11.6‰ (VPDB). The data  
305 indicate that carbon-oxygen isotope systematics of Balkaya samples are higher than Sarıhıdır  
306 carbonates.

307

308

#### 309 **5. Discussion**

##### 310 **5.1. Origin of fossil fluid circulations**

311 Carbon isotope compositions of Balkaya (11.5 to 13.2‰) and Sarıhıdır carbonates (8.7 to  
312 11.0‰) yield similar ranges. These values are higher than the array suggested for the marine  
313 limestones ( $\pm 3\%$ ; Clark and Fritz, 1997) but within the range of meteogene fluids ( $-3$  to  
314  $+8\%$ ; Pentecost, 2005). In a previous study by Karabacak et al. (2017),  $\delta^{13}\text{C}$  values of İhlara  
315 carbonates between the Hasandag volcano and Acıgöl Caldera are reported between 7.64

316 and 9.31‰, which are closely consistent with the values of carbonate veins from Balkaya  
317 and Sarıhıdır sites.

318 As shown from the  $\delta^{13}\text{C}$  vs.  $\delta^{18}\text{O}$  diagram (Figure 4b), the vein systems of Balkaya and  
319 Sarıhıdır sites, although nearly 10 km apart, are represented by different carbon-oxygen  
320 isotope systematics. For example, carbonate samples of locations 1 ( $r^2 = 0.99$ ) and 2 ( $r^2 =$   
321  $0.93$ ) from the Sarıhıdır site show a very strong positive correlation. However, location 4  
322 from the Balkaya area is characterized by a rather low correlation with  $r^2 = 0.61$ . Figure 4b  
323 also implies that heavy isotope enrichment of samples is not restricted only to carbon but  
324 also oxygen isotope. Previous studies show that travertines deposited during rapid  $\text{CO}_2$   
325 degassing resulting from seismic events are enriched in both  $^{18}\text{O}$  and  $^{13}\text{C}$  (e.g. Pentecost,  
326 2005; Uysal et al., 2009; Yıldırım et al., in press). According to Ercan et al. (1995) and Güleç et  
327 al. (2002), mantle-derived He contributed to the thermal fluids in the central Anatolia is  
328 almost 35% of total helium inventory. Therefore, it is likely that volcanism is the major  
329 process accounting for the high volatile inventory of the fluids in this region.  $\delta^{13}\text{C}$  values of  
330 fumaroles ( $\text{CO}_2$  gas) emitting in central Anatolia ( $-1.9\text{‰}$ ) fall in the range of limestones  
331 (Mutlu et al., 2018). The difference between carbon isotope values of fumaroles and  
332 travertines in the region is attributed to  $\text{CO}_2$  degassing from hot springs, which resulted in  
333 carbon isotope fractionation. This gave rise to the participation of heavy carbon isotope ( $^{13}\text{C}$ )  
334 into carbonate phase and enrichment of light carbon isotope ( $^{12}\text{C}$ ) in the gas phase.  
335 Precipitation from isotopically enriched waters explains the isotopically heavy character of  
336 the Balkaya and Sarıhıdır carbonates.

337 Unlike carbon isotopes, oxygen isotopes can be used to estimate the isotope composition  
338 and/or equilibrium temperature of waters that precipitated the carbonates (Friedman and

339 O'Neil, 1977). The temperatures of hot spring issuing in the Sarıhıdır site and a thermal  
340 water produced from a well drilled in the same area are 29<sup>0</sup>C and 44<sup>0</sup>C, respectively.  
341 Assuming that discharge temperatures of thermal waters in the region have not significantly  
342 changed in the studied time interval and using the oxygen isotopic fractionation between  
343 calcite and water ( $\Delta^{18}\text{O}_{\text{calcite-water}}$ ) proposed by Kele et al. (2015), we calculated  $\delta^{18}\text{O}$  values of  
344 waters that precipitated Balkaya and Sarıhıdır carbonate veins (Table S6). Oxygen isotope  
345 composition of fluids at 29<sup>0</sup>C is found in the range of -16.0 to -11.2‰ (average: -13.8‰) for  
346 the Sarıhıdır samples and from -11.2 to -9.1‰ (average: -9.9‰) for the Balkaya samples.  
347  $\delta^{18}\text{O}$  values estimated at 44<sup>0</sup>C are -12.9 to -8.1‰ (average: -10.3‰) and -8.1 to -5.9‰  
348 (average: -6.7‰) for the respective fields. These values indicate a meteoric origin for the  
349 paleowaters.

350 Assessment of temporal variations in oxygen isotope systematics of Balkaya carbonate veins  
351 indicates a significant decrease around 133 ka BP (Figure 6 and Table 2). Nearly 2‰ decline  
352 of  $\delta^{18}\text{O}$  is most probably due to meteoric water influx into the deposition site. It is driven  
353 either by a high rate of dilatation which increased the meteoric water component of fluids or  
354 by an enhanced rainfall event in the Eastern Mediterranean land and sea regions (e.g., Bar-  
355 Matthews et al., 2003).

356 Throughout the late Pleistocene, the Earth has experienced periods of glacial climate  
357 terminations (glacial-to-interglacial transitions) on both orbital and millennial time scales.  
358 The long term changes in orbital parameters have led to quasi-periodic fluctuations in the  
359 eccentricity, obliquity and precession of the equinoxes with frequencies at around 100, 41  
360 and 19/23 ka BP, respectively (e.g. Milankovitch, 1941; Berger, 1978). These quasi-cycles are  
361 originated from astronomically driven changes in the latitudinal and seasonal distributions of

362 the solar energy (Berger and Loutre, 2004). Among these cycles, those recurring every 100-  
363 ka are prominently recorded in atmospheric CO<sub>2</sub> from Vostok (Petit et al., 1999), benthic  
364  $\delta^{18}\text{O}$  from the ocean cores (Martinson et al., 1987; Cortijo et al., 1994), continental ice  
365 sheets in the Northern Hemisphere (Bender et al., 1994) and speleothems throughout the  
366 world (Bar-Matthews et al., 1997; 2003; Drysdale et al., 2009). These variations are widely  
367 accepted to control the commencement of late Pleistocene glacial terminations, which are  
368 found at 23, 139, 253, 345, 419, 546 and 632 ka BP (Schulz and Zeebe, 2006).

369 Termination II among others received intense research over the last two decades as high-  
370 resolution U-series dates became available on carbonate materials for which radiocarbon  
371 dating method is only possible for the last 40-50 ka. Consequently, the beginning of  
372 Termination II was elaborated by a number of studies on speleothems and benthic  
373 carbonates (136 to 129 ka BP; Gallup et al., 2002; Landais et al., 2013). In these studies,  $\delta^{18}\text{O}$   
374 was reported to decrease during warmer (interglacial or interstadial) periods. An attempt is  
375 made here to compare oxygen isotope data on Balkaya carbonate veins with records of  
376 marine benthics (Lisiecki and Raymo, 2005), and speleothems of Soreq cave (Bar-Matthews  
377 et al., 2003), Antro del Corchia cave, (Drysdale et. al, 2005), Kesang cave (Cheng et al., 2012),  
378 Buraca Gloriosa cave (Denniston et al., 2018) (Figure 5). There is a striking similarity between  
379 isotope records of travertines and global benthic and cave compilations. This implies that  
380  $\delta^{18}\text{O}$  values of carbonates deposited under open air conditions are well correlated with  
381 those of marine and subterranean carbonates and therefore they can be used as a proxy for  
382 the climate studies.

383 The diagram depicted in Figure 6 yields two shoulders of  $\delta^{18}\text{O}$  decrease for the carbonate  
384 veins; the first is at 122.3 ka (sample G-3) and another clustering at around 133 ka (samples

385 E-2, F, G-1, G-2 and H-2). These negative anomalies are separated by a relatively cooler  
386 period at 130 ka represented by a 1‰ increase (sample D1). Our data indicate that the  
387 interglacial period which started at 133 ka BP proceeded only 3 ka and then demised at 130  
388 ka BP. This was followed by a deglaciation with a duration of 8 ka (Figure 5). Interstadial  
389 reversals are common for the glacial Termination II. The lag periods between the interglacial  
390 periods are reported 1 ka to 10 ka (e.g. Schulz and Zeebe, 2006; Moseley et al., 2015).

391 Alternatively, high rate of dilatation is another mechanism responsible for depleted  $\delta^{18}\text{O}$   
392 values recorded in the Balkaya travertines. The  $\delta^{18}\text{O}$  of meteoric waters is strongly latitude  
393 dependent and falls in the range of -2 to -20‰ (SMOW) (Craig, 1961; Kendall et al., 1995). It  
394 is reported that during major earthquakes stable isotope ratios measured in groundwater  
395 significantly changed which cannot be explained with water-rock interaction process (e.g.  
396 Claesson et al., 2004; Reddy and Nagabhushanam, 2012; Skelton et al., 2014). These changes  
397 are caused by crustal dilatation associated with stress build-up before the seismic event,  
398 which facilitated different groundwater components to mix. Although similar isotopic  
399 variations are not previously reported in areas of volcanic unrest, it is likely that crustal  
400 deformation or high rate of dilatation during the volcanic activity may increase the rate of  
401 mixing between thermogene and meteoric waters that precipitated the travertine deposits.

402 To test this, we examine oxygen isotope compositions of mineral waters in the Gümüşkent  
403 area (nearly 20 km NW of study area).  $\delta^{18}\text{O}$  values of Gümüşkent springs fall in the range of -  
404 10.5 to -9.71‰ (Afşin, 2002) which are consistent with the estimated average oxygen  
405 isotope composition of fluids (-9.92‰ at 29°C) that formed the Balkaya carbonate veins.  
406 These values are within the range proposed for meteoric waters. It is important to note that  
407 samples with high rate of dilatation have the lowest  $\delta^{18}\text{O}$  values (-10,9‰ for sample G-1)  
408 (Table 2). Assuming that  $\delta^{18}\text{O}$  of springs has remained unchanged in the studied time

409 interval, there might be significant amount of cold water influx to the deposition site of  
410 Balkaya travertines. Although limited data available, among the samples witnessed high  
411 dilatation rate, G2 and H2 are characterized by notably low rare earth element compositions  
412 (Figure 4a). This might indicate rapid ascent of meteoric waters without sufficient interaction  
413 with the host rocks (Yıldırım et al., in press).

414 In regard to texture and crystal size, sample D1 (dated at 130 ka) from the Balkaya travertine  
415 shows quite different mineralogical features. This sample that does not contain any banding  
416 consists of calcites with different sizes (Figure S9). In this sample, needle-shaped small  
417 calcite crystals occur along the cracks (Figure S9). The remarkable heterogeneous  
418 crystallization indicates that the continuous fluid flow with high discharge rate resulted in  
419 carbonate deposition in a turbulent environment.

420 We conclude that although  $\delta^{18}\text{O}$  values of Balkaya travertines fall in a relatively low range,  
421 they show similar trend to climate proxies preserved in different depositional environments  
422 throughout the world. If the climatic variations are neglected, this might indicate that  
423 studied carbonates were precipitated under similar fluid conditions (by means of origin and  
424 pathway) which are represented by high rate of dilatation followed by the invasion of  
425 meteoric waters. In other words, all the samples investigated are the manifestation of  
426 crustal deformation in the region.

427

## 428 **5.2. Manifestation of paleo-eruptions on the carbonate veins**

429 Current deformation of the Central Anatolia measured by GPS studies is not uniform (e.g.,  
430 Aktuğ et al., 2013; Simao et al., 2016). In any case, however, a regional dilatation dominates

431 despite variations in stress directions in the CAVP (Karabacak et al., 2017). Specifically, as  
432 shown by principle strain and horizontal velocity field analyses, a tension stress striking  
433 WNW-ESE is evident around Balkaya and Sarıhıdır sites (e.g., Aktuğ et al., 2013; Simao et al.,  
434 2016). Our field analyses show that both travertine sites set on the dilational jog area along  
435 the same fault zone (i.e. along the CKFZ with 10 km-distance) and all fractures in Balkaya and  
436 Sarıhıdır sites represent notable opening features (Mode I extension fractures). There are no  
437 slickenlines on their planes and no evidence for compressional tectonics. Thus, it is  
438 concluded that the fractures were formed under the tensile stress-normal trending NNE-  
439 SSW in Balkaya and NNW-SSE in Sarıhıdır. However, although carbonate veins in extensional  
440 fractures along the same fault zones indicate close-epicenter paleoearthquakes (Karabacak  
441 et al., 2019), vein precipitation periods favouring a temporary hydrothermal fluid circulation  
442 due to seismic unrest are completely different in both travertine sites. Consequently, it  
443 cannot be asserted that Sarıhıdır and Balkaya fractures are fully controlled by the regional  
444 dominant stress orientations and/or activity of CKFZ, i.e. it requires other mechanisms. One  
445 of the main reasons of Quaternary crustal deformation in the study area is the growth of  
446 magmatic crests and associated eruptions within a fairly close region (i.e. Acıgöl caldera and  
447 Erciyes stratovolcano). Therefore, it is possible to observe the manifestations of crustal  
448 deformations related to eruptive activity in the vicinity of study area. In the volcanic regions,  
449 pressure change at the tip of magma body results in shear and tensile failures or fluid  
450 pressurization (Rubin and Gillard, 1998; Azzarro, 1999; Glen and Ponce, 2002; Zobin, 2003)  
451 and the deformation produces three types of fractures around volcanoes, i.e. radial, cone  
452 sheet and ring types (Anderson, 1951). Inflation/deflation of magma chamber or volcanic  
453 spreading form  $\sigma_3$  in a radial pattern and generate extensional ring fractures (e.g. Anderson,  
454 1951; Macdonald, 1972; Park, 1989; Borgia et al., 2014). This setting forms ideal deep

455 penetrating pathways for fluid circulations during strain cycles. Thus, the extensional  
456 fracture systems aligned tangential to the volcanic conduits could present unique  
457 manifestations of syn-eruptive fluid circulations. For example, Karabacak et al. (2017)  
458 focused on two different fracture systems in the Ihlara site (central Anatolia) and indicated  
459 different fluid migration pathways for each. The dates of carbonates in each system are  
460 correlated well with the eruptive history of the Acigöl caldera and Hasandag stratovolcano.  
461 Assessment of their data indicates that the formation of these fracture systems in the Ihlara  
462 site is controlled by various eruption centers where they are positioned tangentially. If we  
463 consider the geometric setting of the fracture systems, Balkaya and Sarıhıdır carbonate veins  
464 have positioned tangential to the Acigöl caldera and Erciyes stratovolcano, respectively  
465 (Figure 6). Therefore, the correlation of the timing of carbonate precipitation with paleo-  
466 eruption records in CAVP may provide significant supplementary geochronological data.

467 Figure S10a-c displays the U-series age distribution of carbonate veins in the Balkaya and  
468 Sarıhıdır travertine sites. The age data indicate that the vein precipitations clustered in 3  
469 major periods in last 190 ka (i.e. 5-35, 60-100, 120-170 ka BP) (Figure S10c). Accordingly, the  
470 crustal deformation intensified during 2 different periods at about 9, 82 ka BP in Sarıhıdır  
471 (Figure S10a) and during at least 7 different periods at about 15, 22, 73, 94-100, 119, 133,  
472 145-150, 164 ka BP in Balkaya (Figure S10b). Carbonate vein from Location 4 in Balkaya also  
473 presents a detailed continuous precipitation record for the region (Figure S11a). Figure 6a  
474 displays the U-series ages with respect to distance from the vein center to the wall. If we  
475 order the coeval bands, the graph revolves to U-series age vs. the band widths (Figure S11b)  
476 and displays that the vein has 8 rapid dilatation periods at 15, 22, 67-73, 94-100, 119, 133,  
477 145-155, and 164-171 ka BP coherent to picks of relative probability graph (Figure S10b).

478 Figure S10d displays the paleo-eruption dating records in CAVP for the last 190 ka compiled  
479 from the previous studies (Table S1). Results show that the eruptions took place across the  
480 region episodically in 3 major periods (i.e. 5-40, 75-115, 145-190 ka BP) are compatible with  
481 carbonate precipitations around Sarıhıdır and Balkaya (Figure S10c). Accordingly, each  
482 eruptive period in the CAVP lasted approximately 35-45 ka and is followed by an episode of  
483 volcanic unrest of around 30 ka. Comparison of the carbonate precipitation periods (i.e.  
484 intensified crustal deformation periods) with the eruption records in the surrounding area  
485 yields that there is a great affinity between the Sarıhıdır results and Erciyes eruptions and  
486 between the Balkaya results and Acıgöl eruptions. For example, Holocene eruption on  
487 Erciyes Stratovolcano of  $8.8\pm 0.6$  ka BP (Sarıkaya et al., 2006; 2017) was recorded at Sarıhıdır  
488 carbonate veins (sample 04;  $8.8\pm 3.8$  ka BP). Similarly, an eruption dated at  $22.3\pm 1.1$  ka BP in  
489 the Acıgöl Caldera region (Karnıyarık cone, 24 km distant from Balkaya) (Schmitt vd., 2011)  
490 was almost perfectly recorded in the Balkaya site (sample B;  $22.4\pm 2.1$  ka BP). Table 3  
491 summarizes the results of U-Th ages of the carbonate veins respect to the timing of volcanic  
492 eruption events in the surrounding region.

493

494

## 495 **6. Conclusions**

496 In the volcanic regions, while pressure change of magma chamber generates extensional ring  
497 fractures forming ideal deep penetrating pathways for fluid circulations, the extensional  
498 fracture systems positioned tangentially to eruption centers could present manifestations of  
499 fluid circulations during volcanic strain cycles. In the suitable areas, thus, high flux of CO<sub>2</sub>-rich

500 fluid discharge precipitates syn-eruptive carbonate veins in the fractures. Here we propose a  
501 model, carbonate veins of the extensional fracture systems positioned tangentially to a  
502 volcanic conduit provide a substantial late Quaternary paleo-eruption record for that center  
503 (Figure 6).

504  $\delta^{18}\text{O}$  and  $\delta^{13}\text{C}$  values of travertine sites of CAVP are within the range of meteogene fluids.

505 The significant decrease in oxygen isotope values of Balkaya carbonate veins is likely due to meteoric  
506 water influx into the deposition site. It is driven either by a high rate of dilatation that increased the  
507 meteoric water component of fluids or by an enhanced rainfall event triggered by a change in the  
508 climate regime.

509

510

511

## 512 **Acknowledgements**

513 This research is funded by the Scientific and Technological Research Council of Turkey  
514 (TUBITAK) (under grant # 118Y069). Datasets for this research are included in this paper and  
515 its supplementary information files (the references can be found in the paper).

516

517

## 518 **References**

519 Afşin, M. (2002). Hydrogeochemistry of CO<sub>2</sub>-rich Çorak, Karakaya and Gümüşkent mineral  
520 waters in Nevşehir, Earth Sciences, 26,1-14.

521 Aktuğ, B., Parmaksız, E., Kurt, M., Lenk, O., Kılıçoğlu, A., Gürdal, M.A., Özdemir, S. (2013).  
522 Deformation of Central Anatolia: GPS implications, Journal of Geodynamics, 67, 78–  
523 96.

- 524 Altunel, E., Karabacak, V. (2005). Determination of horizontal extension from fissure-ridge  
525 travertines: a case study in the Denizli Basin, southwestern Turkey, *Geodinamica Acta*,  
526 18/3-4 (2005) 333-342.
- 527 Anderson, E.M. (1951). The dynamics of faulting and dyke formation with applications to  
528 Britain, Oliver and Boyd, Edinburgh and London.
- 529 Aydar, E., Gourgaud, A., Deniel, C., Lyberis, N., Gundogdu, N. (1995). Le volcanisme  
530 quaternaire d'Anatolie centrale (Turquie) : Association de magmatisme calco-alkalin et  
531 alcalin en domaine de convergence, *Canadian J. of Earth Science*, 32, 7, 1058-1069.
- 532 Aydar, E., Gundogdu, N., Bayhan, H., Gourgaud, A. (1994). Volcano-structural and  
533 petrological investigation of the Cappadocian Quaternary volcanism, TUBITAK  
534 *Yerbilimleri Dergisi*, 3, 25-42, In Turkish with English abstract.
- 535 Azzaro, R. (1999). Earthquake surface faulting at Mount Etna volcano (Sicily) and implications  
536 for active tectonics, *Journal of Geodynamics*, 28, 193-213.
- 537 Bar-Matthews M., Ayalon A., Kaufman A. (1997). Late Quaternary paleoclimate in the  
538 eastern Mediterranean region from stable isotope analysis of speleothems at Soreq  
539 Cave, Israel. *Quat. Res.* 47, 155– 168.
- 540 Bar-Matthews, M., Ayalon, A, Matthews, M., Gilmour, M., Hawkesworth, C. (2003). Sea-land  
541 oxygen isotopic relationships from planktonic foraminifera and speleothems in the  
542 Eastern Mediterranean region and their implication for paleorainfall during interglacial  
543 intervals. *Geochem. Cosmochim. Acta* 67 (17), 3181-3199.
- 544 Bar-Matthews, M., Ayalon, A., Sass, E., Halicz, L. (1994). Water behaviour in karstic system-  
545 Soreq Cave, Beit-Shemesh, summary of three years study. *Israel Geol. Surv. Rep. #*  
546 *GSI/6/94*.
- 547 Bender, M., Sowers, T., Labeyrie, L.D. (1994). The Dole effect and its variation during the last  
548 130,000 years as measured in the Vostok core. *Glob. Biogeochem. Cycles* 8, 363–376.
- 549 Berardi, G., Vignaroli, G., Billi, A., Rossetti, F., Soligo, M., Kele, S., Baykara, M.O., Bernasconi,  
550 S.M., Castorina, F., Tecce, F., Shenet, C.C. (2016). Growth of a Pleistocene giant  
551 carbonate vein and nearby thermogene travertine deposits at Semproniano, southern  
552 Tuscany, Italy: Estimate of CO<sub>2</sub> leakage, *Tectonophysics*,  
553 <http://dx.doi.org/10.1016/j.tecto.2016.04.014>
- 554 Berger, A. (1978). Long-term variations of daily insolation and quaternary climatic changes *J.*  
555 *Atmospheric Sci.*, 35, 2362-2367.
- 556 Berger, A., Loutre, M.F. (2004). Astronomical theory of climate change. *Journal De Physique*,  
557 IV, 121, 1–35.

558 Bigazzi, G., Yegingil, Z., Ercan, T., Oddone, M., Ozdogan, M. (1993). Fission track dating  
559 obsidians in central and northern Anatolia, *Bull. Volc.*, 55, 588-595.

560 Borgia, A., Mazzoldi, A., Brunori, C.A., Allocca, C., Delcroix, C., Micheli, L., Vercellino, A.,  
561 Grieco, G. (2014). Volcanic spreading forcing and feedback in geothermal reservoir  
562 development, Amiata Volcano, Italia. *J. Volc. Geoth. Res.* 284, 16-31

563 Brogi, A., Capezzuoli, E. (2014). Earthquake impact on fissure-ridge type travertine  
564 deposition, *Geological Magazine*, 151, 1135-1143.

565 Brogi, A., Capezzuoli, E., Kele, S., Baykara, M.O., Shen, C.C. (2017). Key travertine tectofacies  
566 for neotectonics and palaeoseismicity reconstruction: effects of hydrothermal  
567 overpressured fluid injection, *Journal of the Geological Society*, 174(4), 679.

568 Capezzuoli, E., Ruggier, G., Rimondi, V., Brogi, A., Liotta, D., Alçiçek, M.C., Alçiçek, H., Bülbül,  
569 A., Gandin, A., Meccheri, M., Shen, C-C., Baykara, M.O. (2018). Calcite veining and  
570 feeding conduits in a hydrothermal system: Insights from a natural section across the  
571 Pleistocene Gölemezli travertine depositional system (western Anatolia, Turkey),  
572 *Sedimentary Geology*, 364, 180-203.

573 Cheng et al. (2012). The climatic cyclicity in semiarid-arid central Asia over the past 500,000  
574 years. *Geophysical Research Letters*, 39, L01705.

575 Cheng, H., Edwards, R., Hoff, J., Gallup, C., Richards, D., Asmerom, Y. (2000). The half-lives of  
576 uranium-234 and thorium-230, *Chem. Geol.*, 169, 17–33.

577 Claesson, L., Skelton, A., Graham, C., Dietl, C., Mörth, M., Torssander, P., Kockum, I. (2004).  
578 Hydrogeochemical changes before and after major earthquake, *Geology*, 32, 641-644.

579 Clark, I., Fritz, P. (1997). *Environmental isotopes in hydrogeology*. Lewis Publishers, New  
580 York, 328 s.

581 Cortijo, E., Duplessy, J.C., Labeyrie, L., Leclaire, H., Duprat, J., van Weering, T.C.E. (1994).  
582 Eemian cooling in the Norwegian sea and North Atlantic ocean preceding continental  
583 ice-sheet growth. *Nature* 372, 446–449.

584 Craig, H. (1961). Isotopic variations in meteoric waters. *Science* 133, 1702–1703.

585 Denniston, R. F., Houts, A. N., Asmerom, Y., Wanamaker Jr., A. D., Haws, J. A., Polyak, V. J.,  
586 Thatcher, D. L., Altan-Ochir, S., Borowske, A. C., Breitenbach, S. F. M., Ummenhofer, C.  
587 C., Regala, F. T., Benedetti, M. M., Bicho, N. F. (2018). A stalagmite test of North  
588 Atlantic SST and Iberian hydroclimate linkages over the last two glacial cycles. *Climate*  
589 *of the Past*, 14, 12, 1893-1913.

590 Dirik, K., Göncüoğlu, M.C. (1996). Neotectonic characteristics of the Central  
591 Anatolia, *International Geology Review*, 38, 807-817.

- 592 Doğan, U. (2011). Climate-controlled river terrace formation in the Kızılırmak Valley,  
593 Cappadocia section, Turkey: inferred from Ar–Ar dating of Quaternary basalts and  
594 terraces stratigraphy, *Geomorphology* 126: 66–81.
- 595 Doğan-Külahçı, G.D. (2015). Chronological, magmatological and geochemical study of post-  
596 collisional basaltic volcanism in Central Anatolia and its spatio-temporal evolution.  
597 *Earth Sciences*. Université Blaise Pascal - Clermont-Ferrand II.
- 598 Drysdale, R.N., Zanchetta, G., Hellstrom, J.C., Fallick, A.E., Zhao, J.X. (2005). Stalagmite  
599 evidence for the onset of the Last Interglacial in southern Europe at  $129 \pm 1$  ka.  
600 *Geophysical Research Letters*, Vol. 32, L24708, doi:10.1029/2005GL024658.
- 601 Drysdale, R.N., Hellstrom, J., Zanchetta, G., Fallick, A E., Sánchez Goñi, M.F., Couchoud, I.,  
602 McDonald, J., Maas, R., Lohmann, G., Isola, I. (2009). Evidence for obliquity forcing of  
603 glacial Termination II, *Science*, 325, 1527–1531.
- 604 Emre, Ö., Duman, T.Y., Özalp, S., Elmacı, H., Olgun, Ş. (2011a). 1:250000 Scale Active Fault  
605 Map Series of Turkey, Aksaray (NJ 36-7) Quadrangle. Serial Number: 26", General  
606 Directorate of Mineral Research and Exploration, Ankara-Turkey.
- 607 Emre, Ö., Duman, T.Y., Özalp, S., Elmacı, H., Olgun, Ş. (2011b). 1:250000 Scale Active Fault  
608 Map Series of Turkey, Kayseri (NJ 36-8) Quadrangle. Serial Number: 32, General  
609 Directorate of Mineral Research and Exploration, Ankara-Turkey.
- 610 Ercan, T., Matsuda, J.I., Nagao, K., Kita, I. (1995). Noble gas isotopic compositions in gas and  
611 water samples from Anatolia. In: Erler, A., Ercan, T., Bingöl, E., Orcen, S., *Geology of*  
612 *the Black Sea Region: Proc. Int. Symp. on the Geology of the Black Sea Region*, Ankara,  
613 Turkey. General Directorate of Mineral Research and Exploration and the Chambers of  
614 Geological Engineers of Turkey, Ankara, pp. 197– 206.
- 615 Friedman, I., O'Neil, J.R. (1977). *Compilation of Stable Isotope Fractionation Factors of 649*  
616 *Geochemical Interest*. USGS Numbered Series (report), 440- KK, 11 p.
- 617 Gallup, C.D., Cheng, H., Taylor, F.W., Edwards, R.L. (2002). Direct determination of the timing  
618 of sea level change during Termination II, *Science*, 295, 310–313.
- 619 Glen, J.M.G., Ponce, D.A. (2002). Large-scale fractures related to inception of the  
620 Yellowstone hotspot, *Geology*, 30, 7, 647–650.
- 621 Güleç, N., Hilton, D.R., Mutlu, H. (2002). Helium isotope variations in Turkey: relationship to  
622 tectonics, volcanism and recent seismic activities. *Chemical Geology* 187, 129–142.
- 623 Innocenti, F., Mazzuoli, G., Pasquare, F., Radicati Di Brozolo, F., Villari, L. (1975). The  
624 Neogene calcalkaline volcanism of Central Anatolia: geochronological data on Kayseri–  
625 Nigde area, *Geol. Mag.*, 112 (4), 349-360.

- 626 Karabacak, V., Uysal, I.T., Mutlu, H., Ünal-İmer, E., Dirik, R.K., Feng, Y-X., Akiska, S., Aydoğdu,  
627 I., Zhao, J-X. (2019). Are U-Th dates correlated with historical records of earthquakes?  
628 Constraints from co-seismic carbonate veins within the North Anatolian Fault Zone,  
629 *Tectonics*, 38, 7, 2431-2448.
- 630 Karabacak, V., Uysal, I.T., Ünal-İmer, E., Mutlu, H., Zhao, J. (2017). U-Th age evidence from  
631 carbonate veins for episodic crustal deformation of Central Anatolian Volcanic  
632 Province, *Quaternary Science Reviews*, 177, 158-172.
- 633 Kele, S., Breitenbach, S.F.M., Capezzuoli, E., Meckler, A.N., Ziegler, M., Millan, I.M., Kluge, T.,  
634 Deák, J., Hanselmann, K., John, C.M., Yan, H., Liu, Z., Bernasconi, S.M. (2015).  
635 Temperature dependence of oxygen and clumped isotope fractionation in carbonates:  
636 a study of travertines and tufas in the 6–95°C temperature range. *Geochimica et*  
637 *Cosmochimica Acta*, 168, 172–192.
- 638 Kendall, C., Sklash, M.G., Bullen, T.D. (1995). Isotope tracers of water and solute sources in  
639 catchments. In: Trudgill ST (ed) *Solute modeling in catchment systems*. Wiley, New  
640 York, pp 261–303.
- 641 Koçyiğit, A., Doğan, U. 2016. Strike-slip neotectonic regime and related structures in the  
642 Cappadocia region: a case study in the Salanda basin, Central Anatolia, Turkey, *Turkish*  
643 *Journal of Earth Sciences*, 25, 393-417.
- 644 Köksal S. and Göncüoğlu M. C. (2008). Nd Isotopic Characteristics of Some S-, I- and A-type  
645 Granitoids from Central Anatolia, *Turkish J. Earth Sci.*, 17, 111–127.
- 646 Kuzucuoğlu, C., Pastre, J-F., Black, S., Ercan, T., Fontugne, M., Guillou, H., Hatte, C.,  
647 Karabiyikoğlu, M., Orth, P., Turkecan, A. (1998). Identification and dating of tephra  
648 layers from Quaternary sedimentary sequences of Inner Anatolia, Turkey, *Journal of*  
649 *Volcanology and Geothermal Research*, 85, 153-172.
- 650 Landais, A., Dreyfus, G.B., Capron, E., Jouzel, J., Masson-Delmotte, V., Roche, D.M., Prié, F.,  
651 Caillon, N., Chappellaz, J., Leuenberger, M., Lourantou, A., Parrenin, F., Raynaud, D.,  
652 Teste, G. (2013). Two-phase change in CO<sub>2</sub>, Antarctic temperature and global climate  
653 during Termination II. *Nature Geoscience*, 6(12), 1062-1065.
- 654 Lawrence, M.G., Kamber, B.S. (2006). The behaviour of the rare earth elements during  
655 estuarine mixing-revisited, *Mar Chem.* 100,147-161.
- 656 Lisiecki, L.E., Raymo, M.E. (2005). A Pliocene-Pleistocene stack of 57 globally distributed  
657 benthic  $\delta^{18}\text{O}$  records. *Paleoceanography*, Vol. 20, PA1003, doi:10.1029/2004PA001071.
- 658 Macdonald, G.A. (1972). *Volcanoes*, Prentice-Hall, New Jersey

- 659 Martinson, D.G., Pisias, N.G., Hays, J.D., Imbrie, J., Moore, T.C., Shackleton, N.J. (1987). Age  
660 dating and the orbital theory of the ice ages: Development of a high-resolution 0 to  
661 300,000-year chronostratigraphy, *Quat. Res.*, 27(1), 1–29.
- 662 Milankovitch, M. (1941). *Kanon der Erdbestrahlungen und seine Anwendung auf das*  
663 *Eiszeiten Problem*, Roy Serbian Acad. Spec. Pub., vol. 133.
- 664 Montgomery, D.R., Manga, M. (2003). Stream flow and water well responses to earthquakes,  
665 *Science*, 300, 2047-2049.
- 666 Moseley, G.E., Spötl, C., Cheng, H., Boch, R., Min, A., Edwards, E. (2015). Termination-II  
667 interstadial/stadial climate change recorded in two stalagmites from the north  
668 European Alps. *Quat. Sci. Rev.* 127, 229–239.
- 669 Mutlu, H., Atıcı, G., Çınar Durgut, N., Hilton, D.R., Akar, M., Çobankaya, M., 2018, Variations  
670 in gas isotope compositions of thermal fluids in central Anatolia, Turkey, EGU General  
671 Assembly Conference Abstracts 20, 539.
- 672 Notsu, K., Fujitani, T., Ui, T., Matsuda, J., Ercan, T. (1995). Geochemical features of collision-  
673 related volcanic rocks in central and eastern Anatolia, Turkey, *Journal of Volcanology*  
674 *and Geothermal Research*, 64 (1995), 171-192.
- 675 Nuriel, P., Rosenbaum, G., Zhao, J.-X., Feng, Y., Golding, S.D., Villemant, B., Weinberger, R.  
676 (2012). U-Th dating of striated fault planes, *Geology*, 40, 7, 647-650.
- 677 Park, R.G., 1989. *Foundations of structural geology*, 2. edition, Blackie, Glasgow and London.
- 678 Pasquare, G., Poli, S., Vezzoli, I., Zanchi, A. (1988). Continental arc volcanism and tectonic  
679 setting in Central Anatolia, Turkey, *Tectonophysics*, 146, 217-230.
- 680 Pentecost, A. (2005). *Travertine*. Springer Verlag, Berlin Heidelberg, 446 p.
- 681 Petit, J.R., J. Jouzel, D. Raynaud, N.I. Barkov, J. Barnola, I. Basile, M. Bender, et al. (1999).  
682 Climate and atmospheric history of the past 420,000 years from the Vostok ice core,  
683 Antarctica. *Nature*, 399(6735), 429–436.
- 684 Piper, J.D.A., Gürsoy, H., Tatar, O. (2002). Palaeomagnetism and Magnetic Properties of the  
685 Cappadocian Ignimbrite Succession, Central Turkey and Neogene Tectonics of the  
686 Anatolian Collage, *J. of Volcanology and Geothermal Research*, 117 (3-4), 237-262.
- 687 Priewisch, A., Crossey, L.J., Karlstrom, K.E, Polyak, V.J., Asmerom, Y., Nereson, A., Ricketts,  
688 J.W. (2014). U-series geochronology of large-volume Quaternary travertine deposits of  
689 the southeastern Colorado Plateau: Evaluating episodicity and tectonic and  
690 paleohydrologic controls, *Geosphere*, 10, 2, 401–423

691 Rankama, K., Sahama, Th.G. (1950). *Geochemistry*. University of Chicago Press, Chicago, 912  
692 p.

693 Reddy, D.V., Nagabhushanam, P. (2012). Chemical and isotopic seismic precursory signatures  
694 in deep groundwater: Cause and effect, *Applied Geochemistry*, 27, 2348-2355.

695 Rizzo, A.L., Uysal, I.T., Mutlu, H., Ünal-İmer, E., Dirik, K., Yüce, G., Caracausi, A., Italiano, F.,  
696 Misseri, M., Temel, A., Bayari, S., Özyurt, N., Zhao, J-X, Deniz, K. (2019). Geochemistry  
697 of fluid inclusions in travertines from western and northern Turkey: inferences on the  
698 role of active faults in fluids circulation, *Geochemistry, Geophysics, Geosystems*, v. 20,  
699 issue 11, 5473-5498.

700 Roberts, N., Reed, J.M., Leng, M.J., Kuzucuoğlu, C., Fontugne, M., Bertaux, J., Woldring, H.,  
701 Bottema, S., Black, S., Hunt, E., Karabıyıkoglu, M. (2001). The tempo of Holocene  
702 change in the Eastern Mediterranean region: new high-resolution crater-lake sediment  
703 data from central Turkey, *The Holocene*, 11. 6, 721-736.

704 Rubin, A.M., Gillard, D. (1998). Dike-induced earthquakes: Theoretical considerations, *J.*  
705 *Geophys. Res.*, 103, 10017-10030, doi:10.1029/ 97JB03514.

706 Sarıkaya, M.A., Çiner, A., Şen, E., Ersoy, O., Zreda, M. (2017). “Dating young lavaflores with  
707 cosmogenic <sup>36</sup>Cl: an example from the late pleistocene–early holocene Erciyes  
708 monogenetic lava domes in Central Turkey”, EGU General Assembly.

709 Sarıkaya, M.A., Zreda, M., Desilets, D., Çiner, A., Şen, E. (2006). “Correcting for nucleogenic  
710 <sup>36</sup>Cl in cosmogenic <sup>36</sup>Cl dating of volcanic rocks from the Erciyes Volcano, Central  
711 Turkey”, AGU Fall Meeting Abstracts.

712 Schmitt, A.K., Danis, M., Evans, N.J., Siebel, W., Kiemele, E., Aydin, F., Harvey, J.C. (2011).  
713 Acigöl rhyolite field, Central Anatolia (part 1): high-resolution dating of eruption  
714 episodes and zircon growth rates, *Contrib. Mineral Petrol.*, 162, 1215–1231.

715 Schulz, K.G., Zeebe, R.E. (2006). Pleistocene glacial terminations triggered by synchronous  
716 changes in Southern and Northern Hemisphere insolation: the insolation canon  
717 hypothesis. *Earth and Planetary Science Letters*, 249, 326-336.

718 Seed, H.B., Idriss, I.M. (1971). Simplified procedure for evaluating soil liquefaction potential,  
719 *J. Soil Mech. Found. Div.*, ASCE 97, 1249-1273.

720 Sibson, R.H. (1987). Earthquake rupturing as a mineralizing agent in hydrothermal systems,  
721 *Geology*, 15, 701-704.

722 Simao, N.M., Nalbant, S.S., Sunbul, F., Mutlu, A.K. (2016). Central and eastern Anatolian  
723 crustal deformation rate and velocity fields derived from GPS and earthquake data,  
724 *Earth and Planetary Science Letters*, 433, 89–98.

- 725 Skelton, A., Andrén, M., Kristmannsdóttir, H., Stockmann, G., Mörth, C., Sveinbjörnsdóttir,  
726 Á., et al. (2014). Changes in groundwater chemistry before two consecutive  
727 earthquakes in Iceland. *Nature Geoscience*, 7, 752–756.
- 728 Taylor, R.S., McLennan, S.M. (1985). *The Continental crust: its composition and evolution*.  
729 Blackwell. Oxford, p. 312.
- 730 Toksoy-Köksal, F., Köksal, S., Göncüoğlu, M.C., Romer, R.L. (2008). An Approach to the  
731 Central Anatolian (Avanos) Late Mesozoic Magmatism: Petrology of Cogenetic Granitic  
732 and Volcanic Rocks. 61st Geological Congress of Turkey, Ankara, Abstr, p. 247-248.
- 733 Toprak, V. (1994). Central Kızılırmak Fault Zone: Northern margin of Central Anatolian  
734 Volcanics, *Turkish Journal of Earth Sciences*, 3, 29-38.
- 735 Toprak, V., Göncüoğlu, M.C. (1993). Tectonic control on the development of Neogene-  
736 Quaternary Central Anatolian Volcanic Province, Turkey: *Geological Journal*, 28, 357-  
737 369.
- 738 Tuccimei, P., Giordano, G., Tedeschi, M. (2006). CO<sub>2</sub> release variations during the last 2000  
739 years at the Colli Albani volcano (Roma, Italy) from speleothems studies *Earth and*  
740 *Planetary Science Letters*, 243, 449-462.
- 741 Türkecan, A., Kuzucuoğlu, C., Mouralis, D., Pastre, J-F., Atıcı, Y., Guillou, H., Fontugne, M.  
742 (2004). Upper Pleistocene volcanism and palaeogeography in Cappadocia, Turkey,  
743 MTA-CNRS-TÜBİTAK 2001–2003 research programme. Project no:101Y109, MTA report  
744 no. 10652, 180 pp.
- 745 Uysal, I.T., Feng, Y., Zhao, J., Işık, V., Nuriel, P., Golding, S.D. (2009). Hydrothermal CO<sub>2</sub>  
746 degassing in seismically active zones during the late Quaternary. *Chemical Geology* 266  
747 265, 442-454.
- 748 Uysal, I.T., Feng, Y., Zhao, J-X., Altunel, E., Weatherley, D., Karabacak, V., Cengiz, O., Golding,  
749 S.D, Lawrance, M.G., Collerson, K.D. (2007). U-series dating and geochemical tracing of  
750 late Quaternary travertine in co-seismic fissures, *Earth and Planetary Science Letters*,  
751 257, 450-462.
- 752 Uysal, I.T., Feng, Y.-X., Zhao, J.-X., Bolhar, R., Isik, V., Baublys, K.A., Yago, A., Golding, S.D.  
753 (2011). Seismic cycles recorded in late Quaternary calcite veins: geochronological,  
754 geochemical and microstructural evidence, *Earth and Planetary Science Letters*, 303,  
755 84–96.
- 756 Uysal, I.T., Ünal-İmer, E., Shulmeister, J., Zhao, J-X., Karabacak, V., Feng, Y.-X., Bolhar, R.  
757 (2019). Linking CO<sub>2</sub> degassing in active fault zones to long-term changes in water  
758 balance and surface water circulation, an example from SW Turkey, *Quaternary*  
759 *Science Reviews*, 214, 164-177.

- 760 Ünal-İmer, E., Uysal, I.T., Zhao, J.X., Işık, V., Shulmeister, J., İmer, A., Feng, Y.X. (2016). CO<sub>2</sub>  
761 outburst events in relation to seismicity: constraints from micro-scale geochronology  
762 and geochemistry of late Quaternary vein carbonates, SW Turkey, *Geochimica et*  
763 *Cosmochimica Acta*, 187, 21–40.
- 764 Vermeesch, P. (2012). On the visualisation of detrital age distributions. *Chemical Geology*,  
765 v.312-313, 190-194.
- 766 Wang, C.-Y., Wang, C.H., Kuo, C.-H. (2004). Temporal change in groundwater level following  
767 the 1999 (Mw = 7.5) Chi-Chi earthquake, Taiwan, *Geofluids*, 4, 210-220.
- 768 Weinstein, Y., Nuriel, P., Inbar, M., Jicha, B.R., Weinberger, R. (2020). Impact of the Dead  
769 Sea Transform Kinematics on Adjacent Volcanic Activity, *Tectonics*, 39, 1,  
770 e2019TC005645
- 771 Williams, R.T., Goodwin, L.B., Sharp, W.D., Mozley, P.S. (2017). Reading a 400,000-year record of  
772 earthquake frequency for an intraplate fault, *Proceedings of the National Academy of Sciences*,  
773 114, 4983-4898.
- 774 Yıldırım, G., Mutlu, H., Karabacak, V., Uysal, I.T., Dirik, K., Temel, A., Yüce, G., Zhao, J-X. (2020).  
775 Temporal changes in geochemical-isotopic systematics of the late Pleistocene Akkaya  
776 travertines (Turkey) - Implications for fluid flow circulation and seismicity, *Chemie der Erde*  
777 (*Geochemistry*), doi: 10.1016/j.chemer.2020.125630
- 778 Zhao, J.-X., Hu, K., Collerson, K.D., Xu, H. (2001) Thermal ionization mass spectrometry U-series  
779 dating of a hominid site near Nanjing, China, *Geology*, 29, 27–30.
- 780 Zobin, V.M. (2003). *Introduction to Volcanic Seismology* (Vol. 6 of *Developments in*  
781 *Volcanology*). Amsterdam: Elsevier.

782

783

## 784 **Figure Captions**

785 **Figure 1.** a. Generalized tectonic setting of the Anatolian Block (yellow arrows show the  
786 plate motions). b. Shaded relief map of the Central Anatolian Volcanic Province  
787 (generated using the WorldImagery data merged to SRTM-3arc-  
788 second resolution digital data) (black lines show the Quaternary faults, blue circles show

789 Neogene activity while the yellow circles show Quaternary activity on stratovolcanoes). B:  
790 Balkaya site, S: Sarıhıdır site, I: Ihlara site.

791 **Figure 2.** Geological setting of the study area and locations of the travertine sites (simplified  
792 from Köksal and Göncüoğlu, 1997; Koçyiğit and Doğan, 2016 and authors' field observations)  
793 (base map is taken from GoogleEarth). Red line indicates the trace of the faults.

794 **Figure 3.** A representative thin section from the carbonates (sample A-2, location 4,  
795 Balkaya). The discontinuities in between the bands (hiatus) are noticeable (yellow lines).  
796 Arrows show the elongation of calcite fabrics (red lines indicate microcrystalline, blue lines  
797 indicate macrocrystalline) (right image is cross-polarized, while the image at the left is plane-  
798 polarized). Note that, we drilled preferentially microcrystalline parts for dating.

799 **Figure 4.** a. PAAS normalized NTE+Y patterns of Balkaya and Sarıhıdır carbonate samples and  
800 host rocks (Taylor and McLennan, 1985) (host rock data from Toksoy-Köksal et al., 2008). b.  
801  $\delta^{18}\text{O}$  vs.  $\delta^{13}\text{C}$  systematics for Balkaya and Sarıhıdır carbonate samples (blue cross: location  
802 1, red cross: location 2, red circle: location 3, blue circle: location 4).

803 **Figure 5.** Comparison of oxygen isotope data on Balkaya carbonate veins with various  
804 climate records. Marine benthic record (Lisiecki and Raymo, 2005), Soreq cave, Israel (Bar-  
805 Matthews et al., 2003), Antro del Corchia cave, Italy (Drysdale et. al, 2005), Buraca Gloriosa  
806 cave, Portugal (Denniston et al., 2018), Kesang cave, China (Cheng et al., 2012).

807 **Figure 6.** Model on correlations of carbonate veins with the paleo-eruption records in the  
808 meaning of fractural positioning to the eruption centers in CAVP. B: Balkaya travertine site,  
809 S: Sarıhıdır travertine site, I: Ihlara travertine site.

810

811 **Table Captions**

812 **Table 1.** The cycle of episodic carbonate vein (banded) precipitation in tectonically active  
813 areas: fluid-rock interaction (modified from Karabacak et al., 2019).

814 **Table 2.** Geochronologic and stable isotope data.

815 **Table 3.** Comparison between the carbonate ages investigated in the study area and the  
816 volcanic eruption events in the surrounding region from the literature.

817

**Figures.**

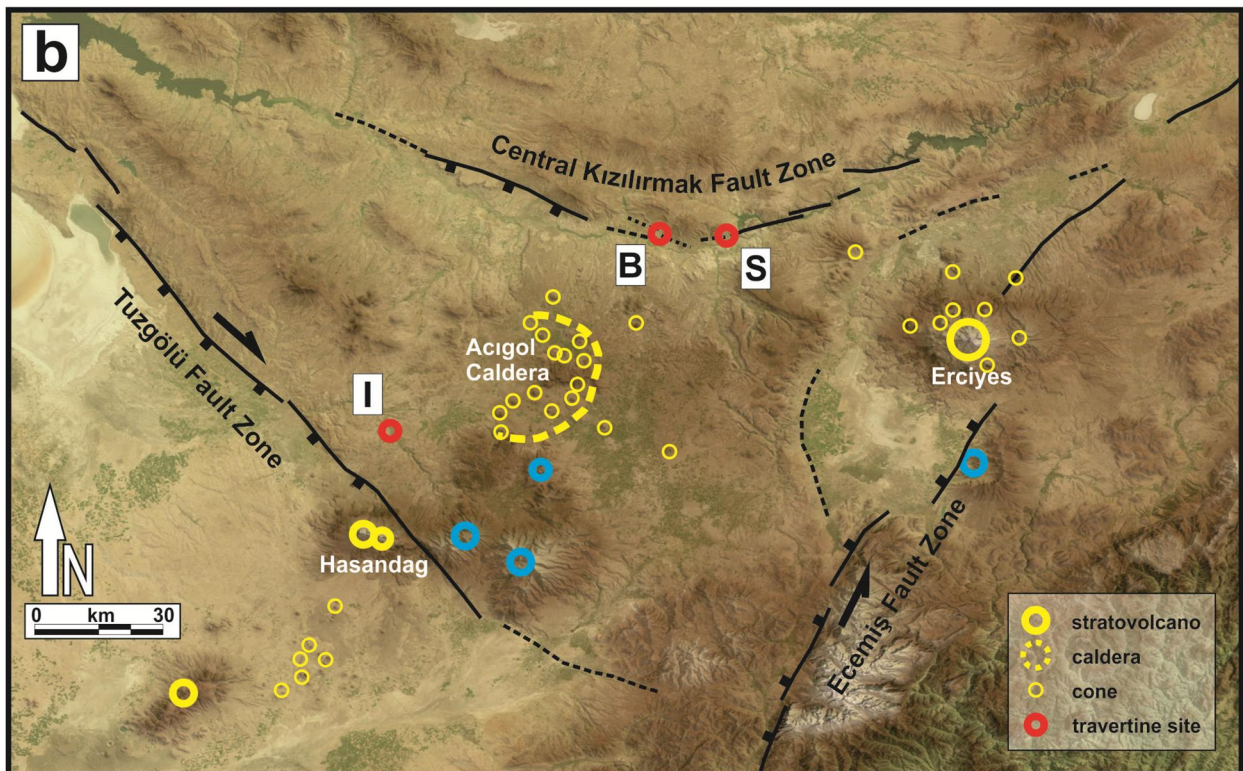
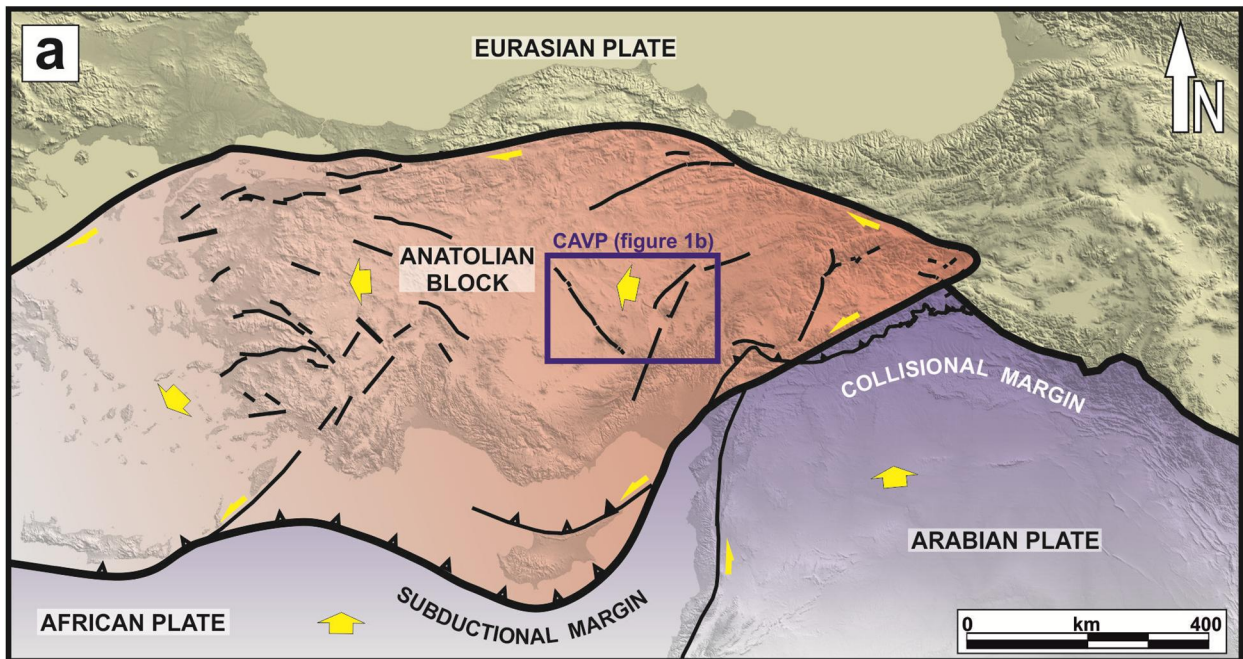


Figure 1

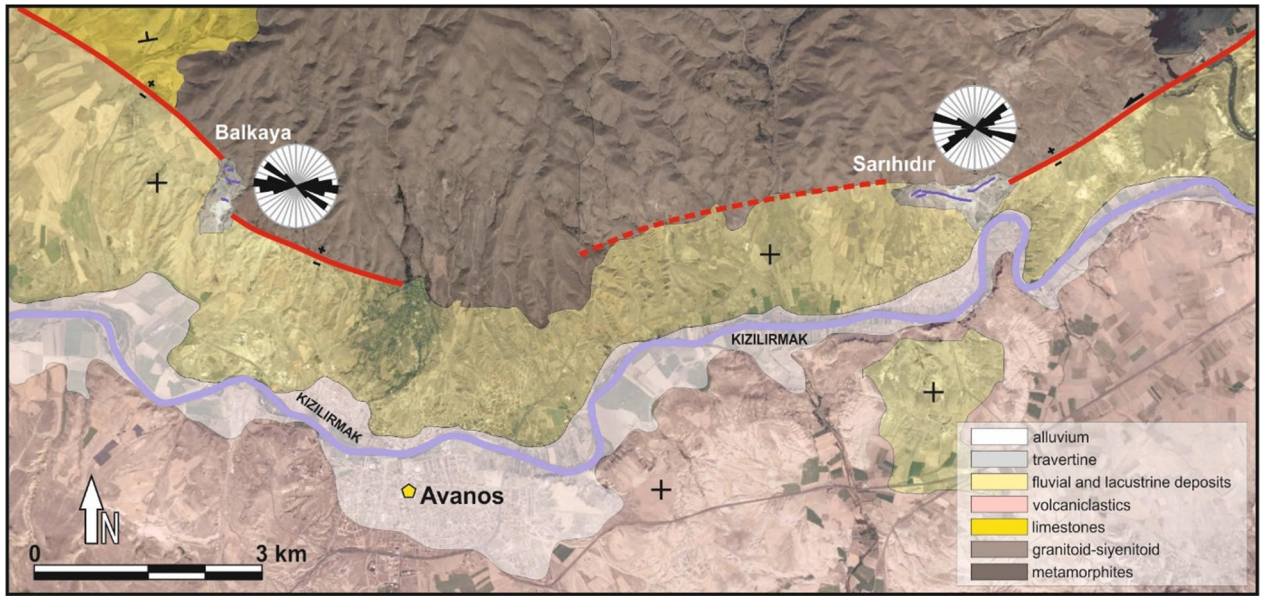


Figure 2.

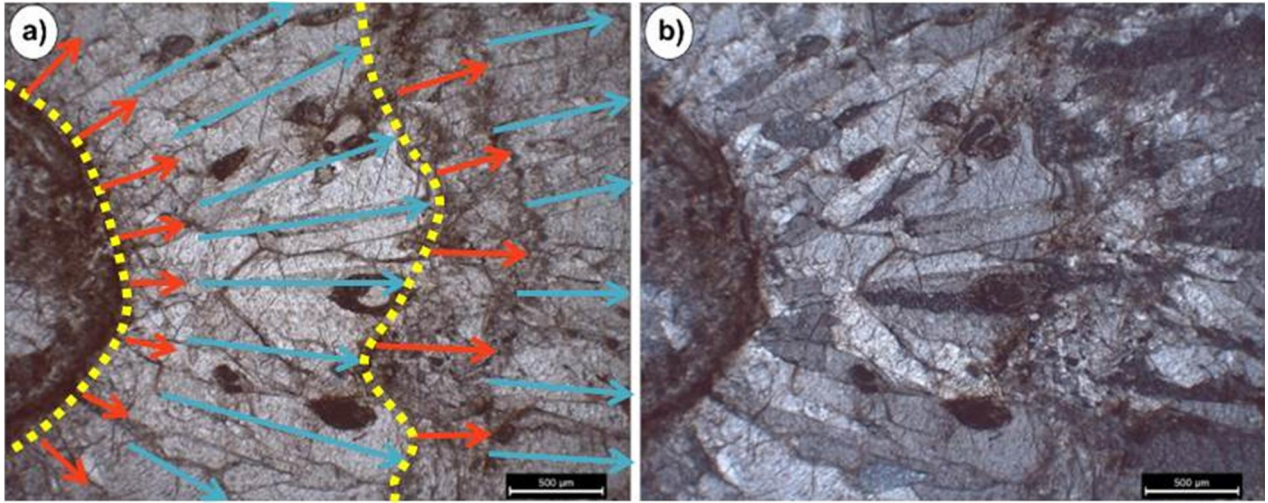


Figure 3.

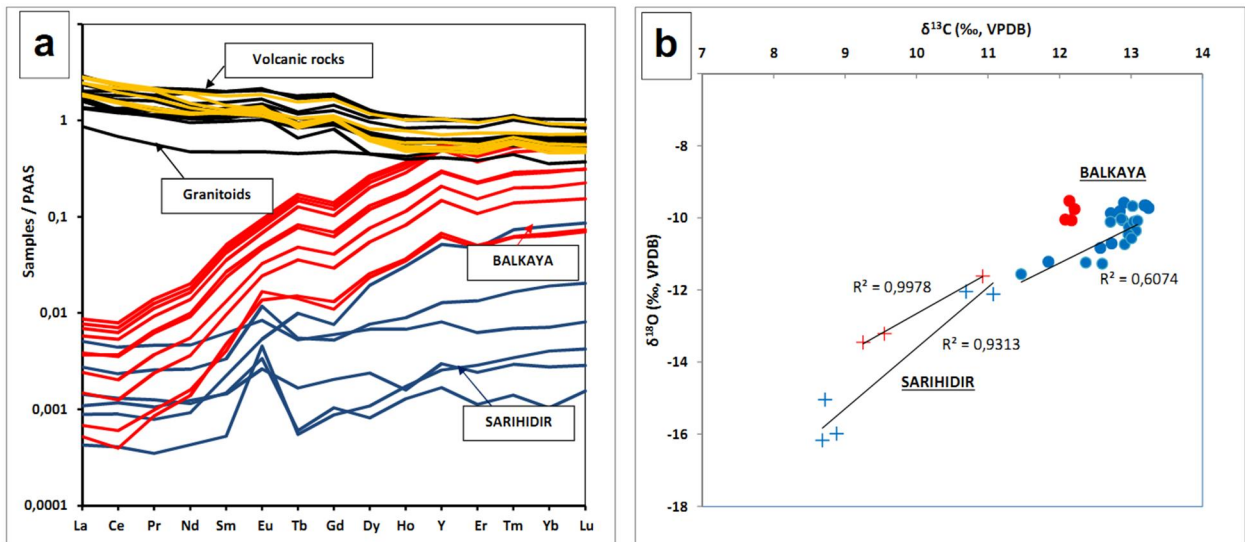


Figure 4.

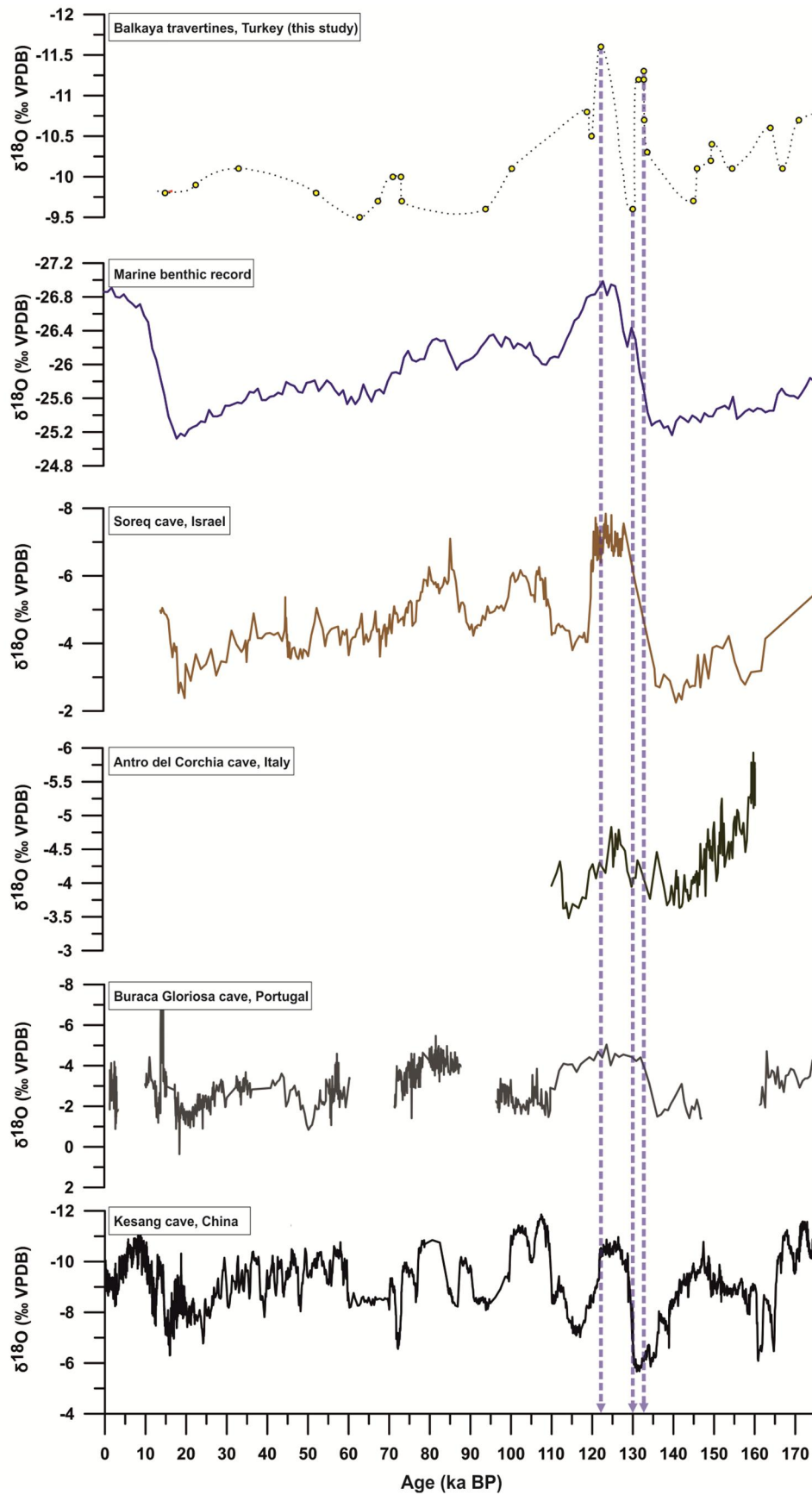


Figure 5.

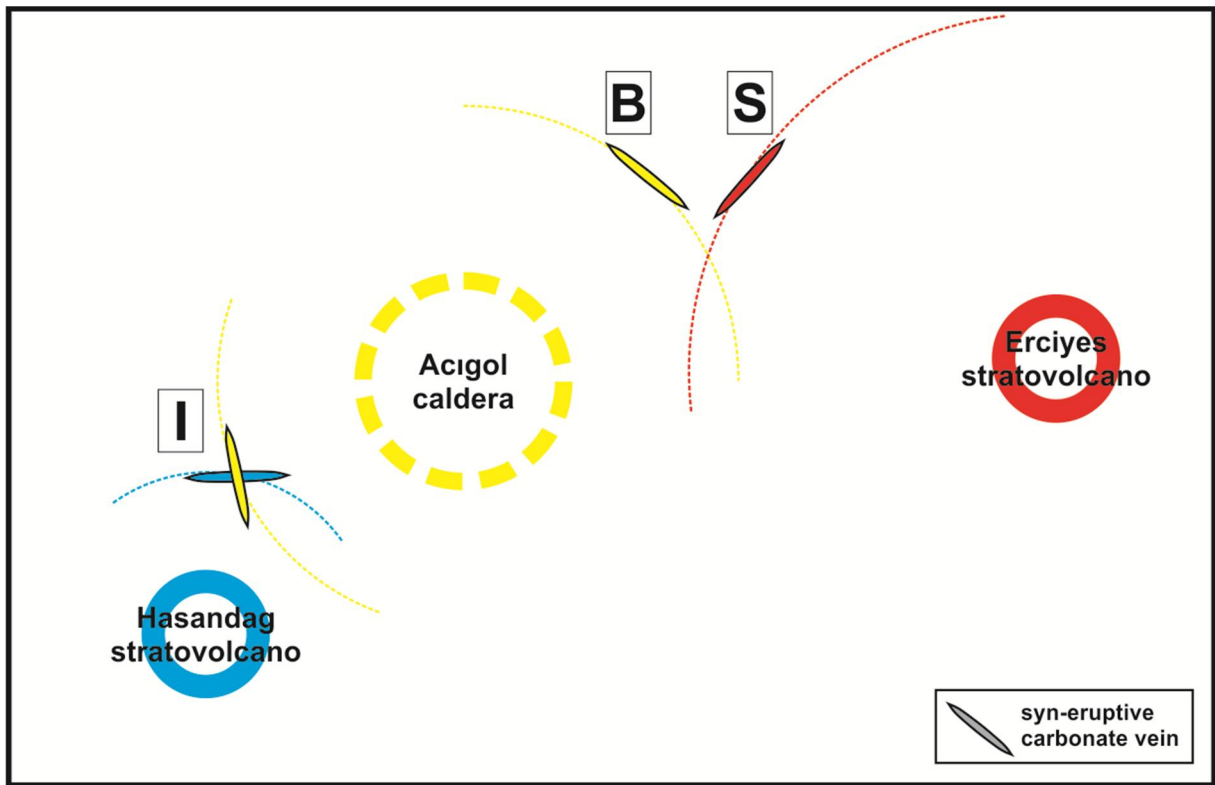


Figure 6.

**Table 1.** The cycle of episodic carbonate vein (banded) precipitation in tectonically active areas: fluid-rock interaction (modified from Karabacak et al., 2019).

period	event	result		evidence
coseismic	seismic release	opening/reopening of fractures		
	simultaneous fluid circulation in fracture systems and expulsion of depressurized/supersaturated hot water	single carbonate band	rapid precipitation of banded carbonate on both walls of the fracture (planar)	whitish microcrystalline calcite that is related to abundant fluid inclusions with high-CO <sub>2</sub> degassing
postseismic	saturated but relatively slow fluid flow		plugging of the fracture along the carbonate vein	light-transparent macrocrystalline calcites that are precipitated at slow degassing rates during the time up to sealing
interseismic	unsaturated and slow fluid flow	shifting spring points (pipes) along the sealed fracture		hiatus (no precipitation)

**Table 2.** Geochronologic and stable isotope data.

site	location	sample	corr. age (ka)	±2s	δ <sup>13</sup> C (VPDB)	δ <sup>18</sup> O (VPDB)	δ <sup>18</sup> O (VSMOW)
SARIHIDIR	1	01	29	50	10,7	-12,0	18,5
		02	8,4	5,7	8,9	-16,0	14,5
		03	11,3	6,0	8,7	-15,0	15,5
		04	8,8	3,8	8,7	-16,2	14,3
		05	7,5	9,8	11,1	-12,1	18,4
	2	06-1	82	121	9,3	-13,4	17,1
		06-2	66	39	10,9	-11,6	18,9
		06-3	81	16	9,5	-13,2	17,3
BALKAYA	3	11A	52,1	8,4	12,2	-9,8	20,7
		11B	62,8	8,4	12,1	-9,5	21,0
		12C	33	10	12,2	-10,1	20,4
		12D	73	13	12,1	-10,0	20,5
	4	A-1	67,3	5,6	13,2	-9,7	20,8
		A-2	14,9	3,2	12,8	-9,8	20,7
		B	22,4	2,1	12,7	-9,9	20,6
		C-1	93,8	3,9	13,2	-9,6	20,9
		C-2	73,2	2,6	13,2	-9,7	20,8
		D-1	130,1	4,9	12,9	-9,6	20,9
		D-2	100,3	3,2	12,9	-10,1	20,4
		E--1	118,8	2,9	12,6	-10,8	19,7
		E--2	132,9	2,7	12,7	-10,7	19,8
		F	132,8	3,9	11,8	-11,2	19,3
		G-1	132,8	3,5	12,6	-11,3	19,2
		G-2	131,5	2,1	12,4	-11,2	19,3
		G-3	122,3	1,1	11,5	-11,6	18,9
		H-1	149,3	7,5	13,0	-10,2	20,3
		H-2	133,6	3,5	13,0	-10,3	20,2
		H-3	154,6	6,0	13,0	-10,1	20,4
		H-4	149,6	5,8	13,1	-10,4	20,1
		H-5	119,9	8,7	13,0	-10,5	20,0
		H-6	171	18	12,9	-10,7	19,8
		H-7	164	27	13,0	-10,6	19,9
		I-1	167	15	13,1	-10,1	20,4
		I-2	145	10	13,0	-9,7	20,8
		J-1	71	15	12,9	-10,0	20,5
		J-2	146	15	12,7	-10,1	20,4

**Table 3.** Comparison between the carbonate ages investigated in the study area and the volcanic eruption events in the surrounding region from the literature.

U-series age data of studied carbonates			volcanic events dated around the study area		
site	sample	corr. age (ka BP)	eruption date (ka BP)	eruption center and evidence	reference
BALKAYA	A-2	14,9±3,2	14	Acıgöl - sediment cores in the late Pleistocene Eski Acıgöl maar, tephra layer (radiocarbon)	Kuzucuoglu et al., 1998
			16	Acıgöl - Acıgöl maar (U-Th)	Roberts et al., 2001
	B	22,4±2,1	22,3±1,1	Acıgöl - Karnıyarık, rhyolitic lava nearly aphyric (U-Th/He)	Schmitt et al., 2011
	12c	33±10	32±3*	Acıgöl - south of Kocadağ (K-Ar)	Türkecan et al., 2004
	12d	73±13	75	Acıgöl - Taşkesik Hill, lava dome	Bigazzi et al., 1993
	C-2	73,2±2,6			
	C-1	93,8±3,9	93±2*	Acıgöl - Boğazköy (obsidian)	Türkecan et al., 2004
	D-2	100,3±3,2	96,0±13,0	Acıgöl - basaltic lava (Karnıyarık Hill) (Ar-Ar)	Doğan, 2011
	E-1	118,8±2,9	117±4	Acıgöl - Alacasar, rhyolitic pumice aphyric (U-Th/He)	Schmitt et al., 2011
	H-5	119,9±8,7			
	I-2	145±10	147±8*	Acıgöl - Taşkesik Hill, rhyolitic lava nearly aphyric (U-Th/He)	Schmitt et al., 2011
	J-2	146±15			
	H-1	149,3±7,5			
	H-4	149,6±5,8			
H-7	164±27	163±7	Acıgöl - upper Acıgöl tuffs Boğazköy, rhyolitic pumice aphyric (U-Th/He)	Schmitt et al., 2011	
I-1	167±15				
SARIHIDIR	05	7,5±9,8	7,2±0,9	Erciyes - lava-flow (Karagüllü) (cosmogenic <sup>36</sup> Cl)	Sarıkaya et al., 2017
			7,7±0,4	Erciyes - lava-flow (Perikartın) (cosmogenic <sup>36</sup> Cl)	Sarıkaya et al., 2017
	02	8,4±5,7	8,8±0,6	Erciyes - lava-flow (Dikkartın) (cosmogenic <sup>36</sup> Cl)	Sarıkaya et al., 2017
	04	8,8±3,8			
	03	11,3±6,0	13±5	Erciyes - cinder cone basalt (K-Ar)	Doğan-Külahcı, 2015
	06-03	81±16	80±10	Erciyes - augite-hypersthene andesite, lava-flow (Karigtepe) (K-Ar)	Notsu et al., 1995
	06-01	82±121			

\* the eruptions of Acıgöl caldera dated from carbonate veins of Ihlara travertine site (Karabacak et al., 2017).